Supplement of Atmos. Chem. Phys., 23, 8789–8804, 2023
https://doi.org/10.5194/acp-23-8789-2023-supplement
© Author(s) 2023. CC BY 4.0 License.

Atmospheric Chemistry and Physics
Open Access

Supplement of

A dynamic parameterization of sulfuric acid–dimethylamine nucleation and its application in three-dimensional modeling

Yuyang Li et al.

Correspondence to: Bin Zhao (bzhao@mail.tsinghua.edu.cn) and Jingkun Jiang (jiangjk@tsinghua.edu.cn)

The copyright of individual parts of the supplement might differ from the article licence.

1 Lookup table for necessary parameters

Table S1. Lookup table for $G(i,j)$ and $H(i)$ in the parameterization

$G(i,j)$		i						
		1	2	3	4	5	6	7
j	1	0.71	0.96	0.86	0.91	1.01	1.15	1.28
	2	0.96	1.20	1.20	1.31	1.47	1.70	1.90
	3	0.86	1.20	1.00	1.01	1.11	1.22	1.32
	4	0.91	1.31	1.01	0.99	1.06	1.13	1.20
	5	1.01	1.47	1.11	1.06	1.12	1.18	1.24
	6	1.15	1.70	1.22	1.13	1.18	1.20	1.24
	7	1.28	1.90	1.32	1.20	1.24	1.24	1.26
$H(i)$		1.00	0.89	0.63	0.51	0.43	0.34	0.29

2 Derivation of the Explicit Formula

Based on the kinetic model presented by Cai et al. (Cai et al., 2021), the formula of pseudo-steady-state cluster concentrations and nucleation rates is as follows:

$$[A_1B_1]=[\mathrm{SA_{tot}}]-[A], \tag{S1}$$

$$[A_1B_1]=\frac{\beta_{1\text{-}2}[A][B]}{\beta_{1\text{-}3}[A]+\beta_{3\text{-}3}[A_1B_1]+\beta_{3\text{-}5}[A_2B_2]+\beta_{3\text{-}6}[A_3B_3]+\beta_{3\text{-}7}[A_4B_4]+\mathrm{CoagS_3}+\gamma}, \tag{S2}$$

$$[A_2B_1]=\frac{\beta_{1\text{-}3}[A][A_1B_1]}{\beta_{2\text{-}4}[B]+\mathrm{CoagS_4}}, \tag{S3}$$

$$[A_2B_2]=\frac{\frac{1}{2}\beta_{3\text{-}3}[A_1B_1][A_1B_1]+\beta_{2\text{-}4}[A_2B_1][B]}{\beta_{3\text{-}5}[A_1B_1]+\beta_{5\text{-}5}[A_2B_2]+\mathrm{CoagS_5}}, \tag{S4}$$

$$[A_3B_3]=\frac{\beta_{3\text{-}5}[A_2B_2][A_1B_1]}{\beta_{3\text{-}6}[A_1B_1]+\mathrm{CoagS_6}}, \tag{S5}$$

$$[A_4B_4]=\frac{\beta_{3,\,6}[A_3B_3][A_1B_1]+\frac{1}{2}\beta_{5,\,5}[A_2B_2][A_2B_2]}{\beta_{3,\,7}[A_1B_1]+\mathrm{CoagS_7}}, \tag{S6}$$

$$J_{A_4B_4}=\beta_{3,\,6}[A_3B_3][A_1B_1]+\frac{1}{2}\beta_{5,\,5}[A_2B_2][A_2B_2], \tag{S7}$$

where $[\mathrm{SA_{tot}}]$ represents the concentrations of sulfuric acid (SA) molecules or clusters containing one SA molecule, A is SA molecules, B is dimethylamine (DMA) molecules, and A_mB_n is the clusters consisting of m SA molecules and n DMA molecules. $\beta_{i\text{-}j}$ ($m^3\ s^{-1}$) represents the collision coefficients (β) between molecules or clusters i and j, and 1-7 represent A, B, A_1B_1, A_2B_1, A_2B_2, A_3B_3, and A_4B_4, respectively. Similarly, CoagS_i represents the coagulation sinks of molecules or clusters i. γ (s^{-1}) is the evaporation rate of A_1B_1 clusters. Here the concentrations of clusters are shown as $[A_mB_n]$ in m^{-3}.

The analytical solution should be simplified based on proper approximations. For typical polluted urban areas, the sink of A_1B_1 is mainly due to the coagulation scavenging and evaporation, that is,

$$[A_1B_1]\approx\frac{\beta_{1\text{-}2}[A][B]}{\mathrm{CoagS_3}+\gamma}, \tag{S8}$$

however, for a wider range of atmospheric environments with lower CS and temperatures, the above approximations might lead to an overestimation of SA-DMA nucleation rates. Thus in this study, the self-coagulation of A_1B_1 and coagulation with A would also be taken into account as a sink of A_1B_1:

$$[A_1B_1]\approx\frac{\beta_{1\text{-}2}[A][B]}{\beta_{1\text{-}3}[A]+\beta_{3\text{-}3}[A_1B_1]+\mathrm{CoagS_3}+\gamma}\approx\frac{\beta_{1\text{-}2}[A][B]}{\beta_{1\text{-}3}[\mathrm{SA_{tot}}]+\mathrm{CoagS_3}+\gamma}, \tag{S9}$$

Putting the above assumption together with the pseudo-steady-state nucleation rates formula, the explicit formula could be simplified to the version in the main text (Eqs. 8-11).

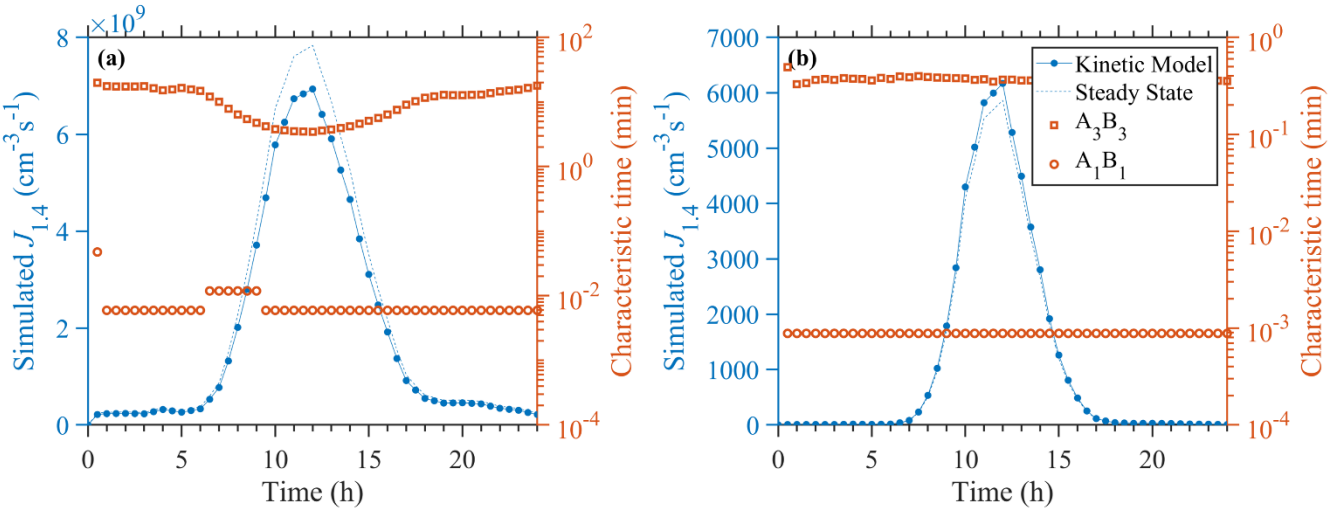

Figure S1. Simulated $J_{1.4}$ (blue) and characteristic equilibrium time (red) of A_3B_3 and A_1B_1. The typical conditions are [DMA]=3.0 pptv with *CS*=0.0001 s^{-1} and *T*=255 K in (a) and *CS*=0.01 s^{-1} and *T*=315 K in (b). The variation of SA concentrations is equal to the averaged diurnal variations.

3 Dimethylamine Emission inventory for marine area

Similar to the continental emission inventory for DMA, the maritime part is also built by combination of NH_3 emission inventory and DMA/NH_3 emission ratio. The maritime NH_3 emission is adopted from the results of Paulot et al with a grid transformation. The DMA/NH_3 emission ratio is estimated by the measured data from a previous study (Chen et al., 2021). During their maritime campaign, mean gaseous DMA and NH3 concentrations are 0.006 μg cm^{-3} and 0.5300 μg cm^{-3}, of which 16% and 34% come from continental transport, respectively. Hence we can obtain the marine-originated DMA (0.0050 μg cm^{-3}) and NH_3 (0.34980 μg cm^{-3}) concentrations and an approximate DMA/NH_3 emission ratio of 0.0144.

Table S2. Key parameters in simulating atmospheric sinks of dimethylamine

Sinks	This study	Variation range
Wet deposition (Henry Law's constant/mol m^{-3} Pa^{-1})	0.56	0.3-0.6 (Sander, 2015)
Gas-phase reaction (•OH oxidation rate constant/cm^{-3} s^{-1})	6.49×10^{-11}	$(5.85\text{-}7.13) \times 10^{-11}$ (Carl and Crowley, 1998)
Aerosol uptake (Uptake coefficient)	0.001	5.9×10^{-4}-4.4×10^{-2} (Qiu et al., 2011; Wang et al., 2010)

4 Dependence of NPF occurrence in 3-D simulation results on CS

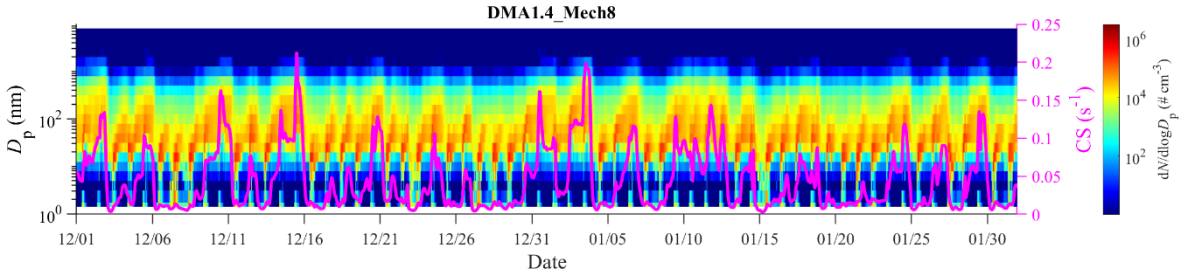

Figure S2. Simulated Evolution of PNSDs and Timeseries of CS (violet line) from scenario DMA1.4_Mech8.

5 Comparisons of simulations between DMA1.4_Mech8 and the scenario with a previous parameterization

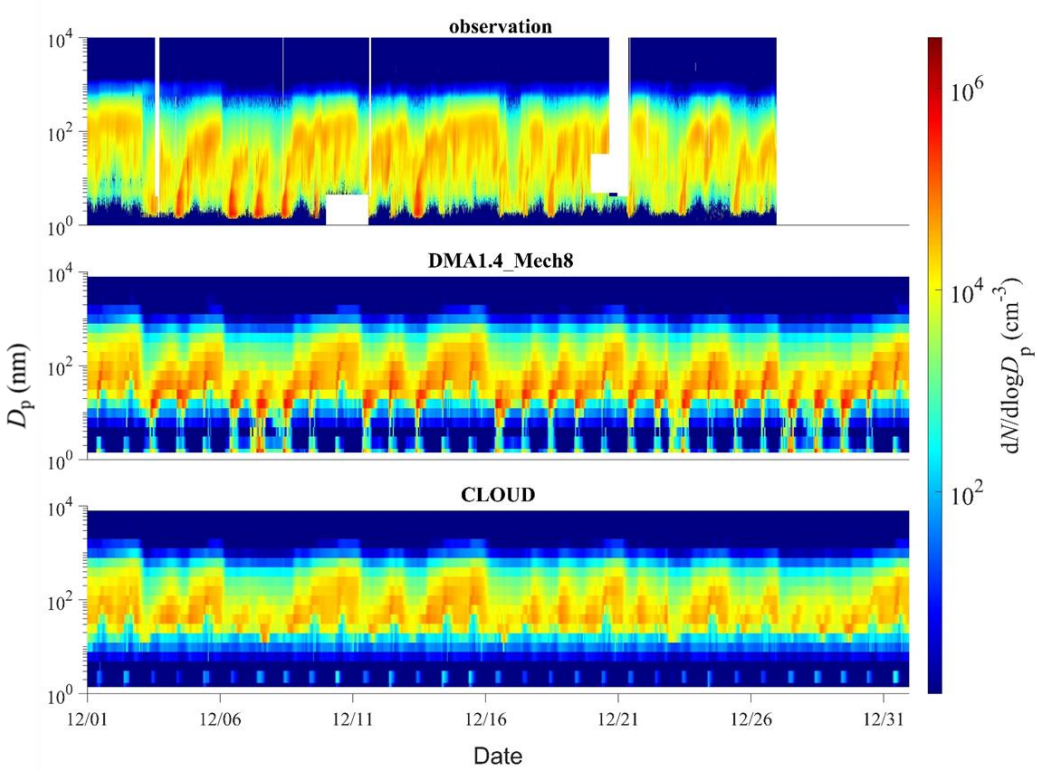

Figure S3. Comparison of observed and simulated averaged particle number size distribution from scenarios with parameterizations from Dunne et al., 2016 (CLOUD) the original scenario (DMA1.4_Mech8).

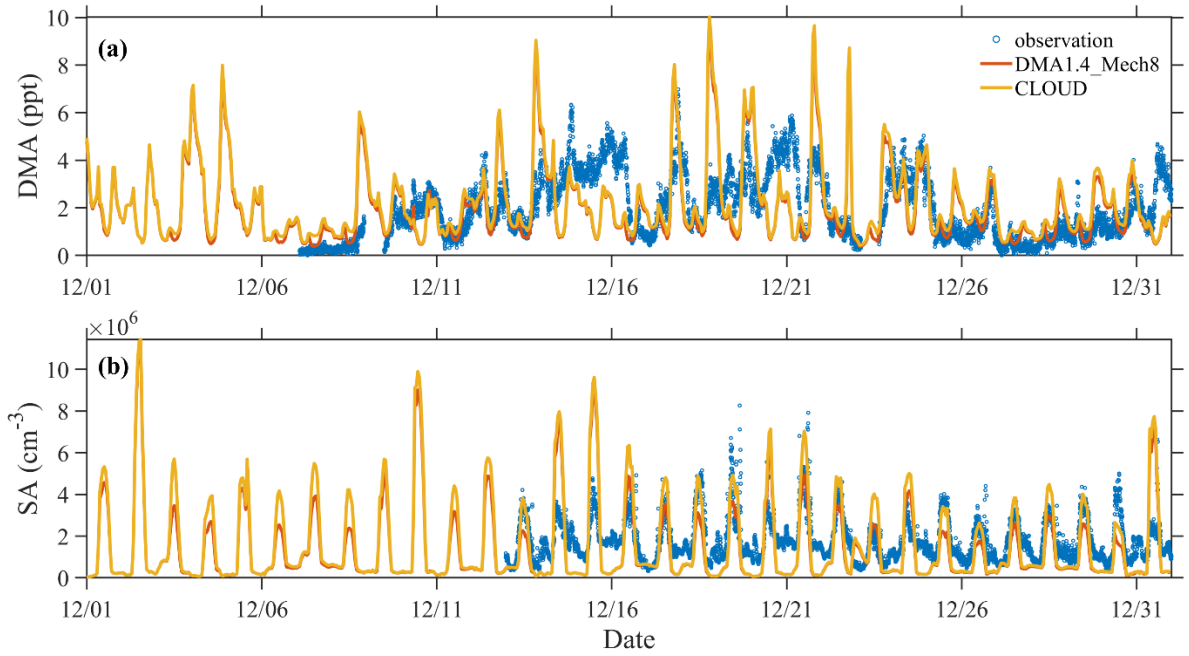

Figure S4. Comparison of observed and simulated DMA (a) and SA (b) concentrations from scenarios with parameterizations from Dunne et al., 2016 (CLOUD) the original scenario (DMA1.4_Mech8).

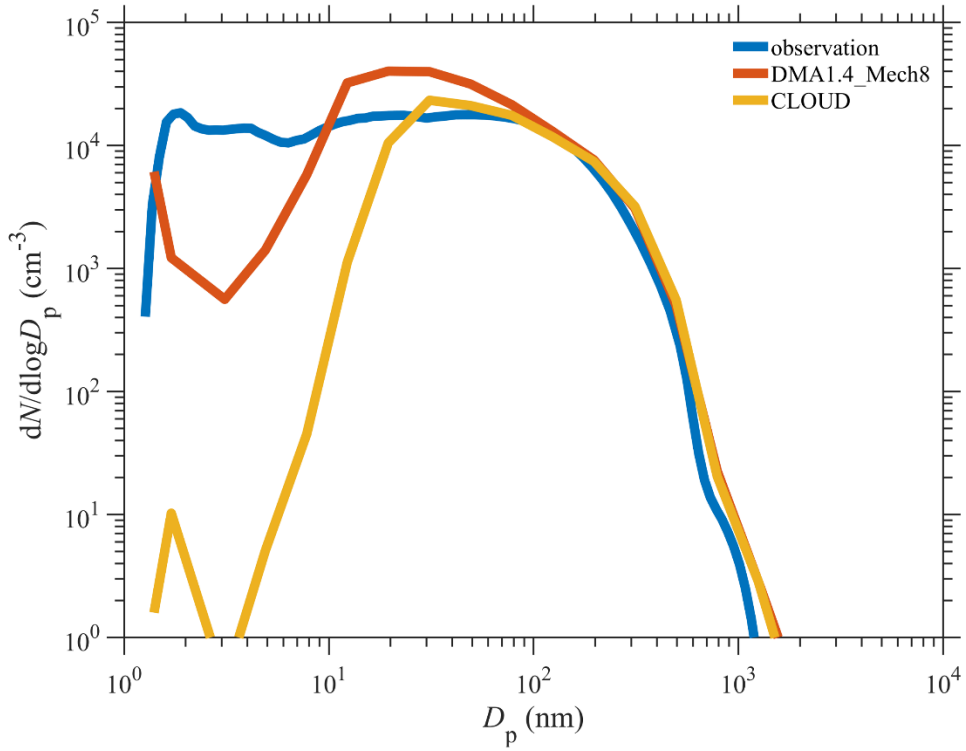

77

78 **Figure S5. Comparison of observed and simulated averaged particle number size distribution from scenarios with**
79 **parameterizations from Dunne et al., 2016 (CLOUD) the original scenario (DMA1.4_Mech8).**

80

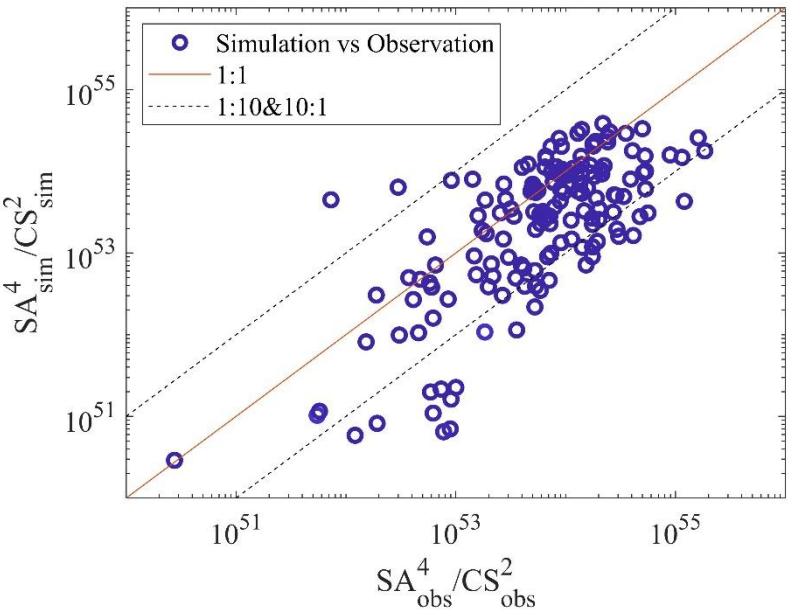

81

82 **Figure S6. Comparison of observed and simulated $[SA]^4/CS^2$ to show the combined effect of simulated input parameters**
83 **in DMA1.4_Mech8.**

84

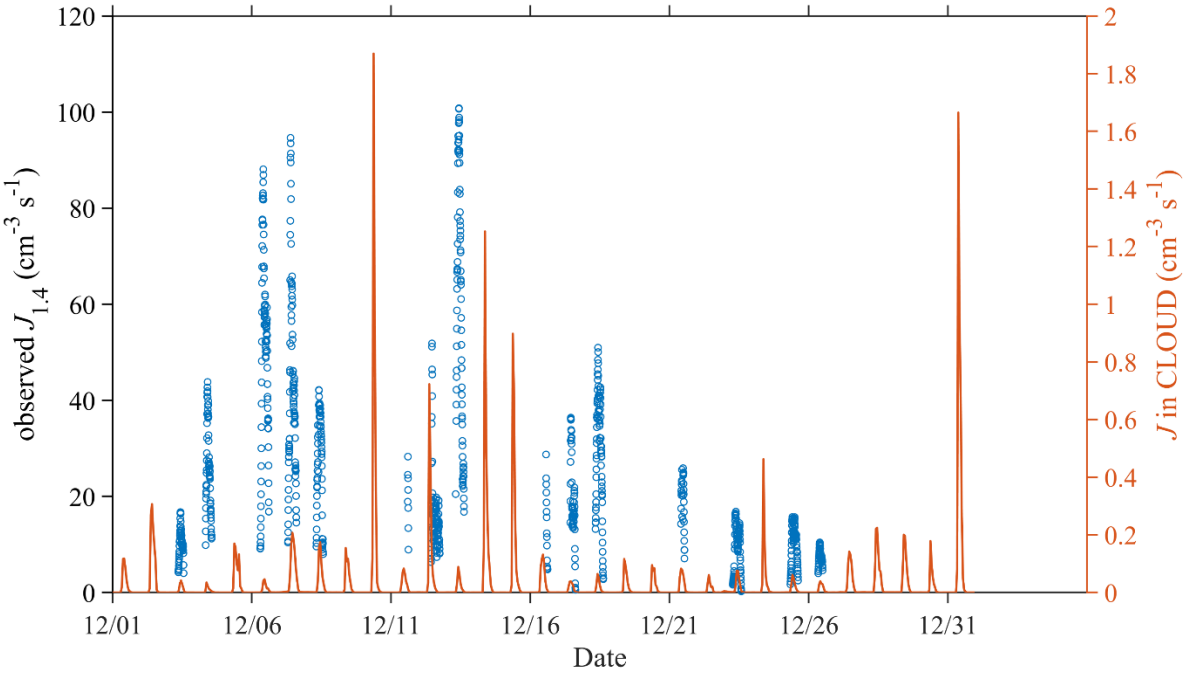

Figure S7. Comparison of observed $J_{1.4}$ and simulated nucleation rates from scenarios with parameterizations from Dunne et al., 2016 (CLOUD).

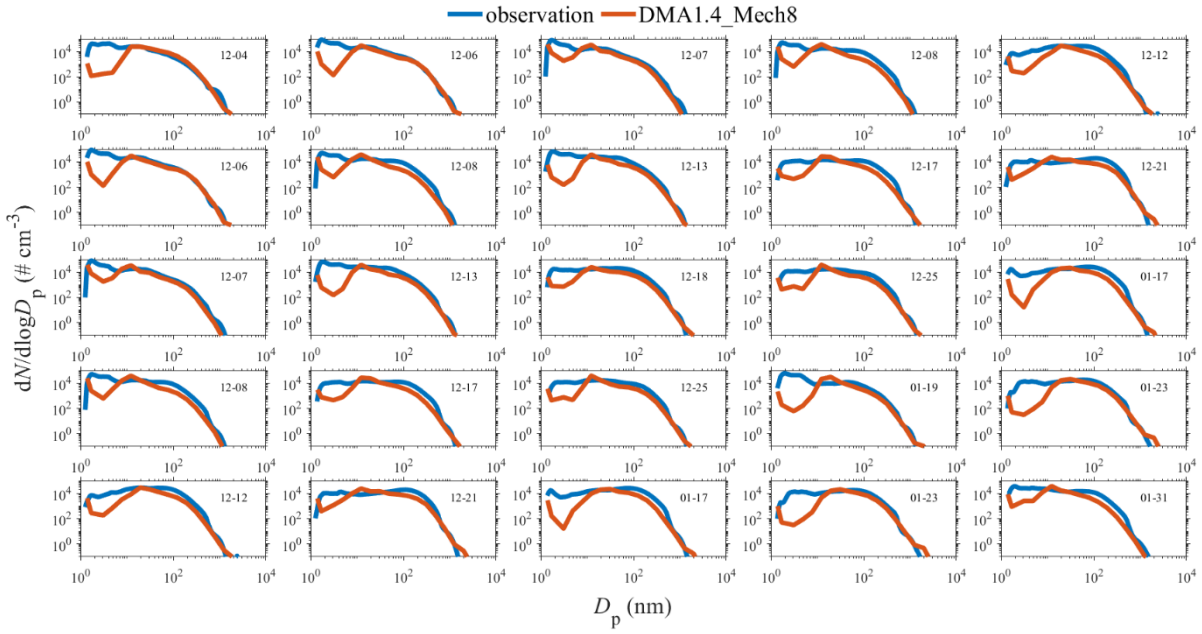

Figure S8. Comparison of observed and simulated averaged particle number size distribution (from DMA1.4_Mech8 scenario) for 25 NPF days.

6 Sensitivity tests

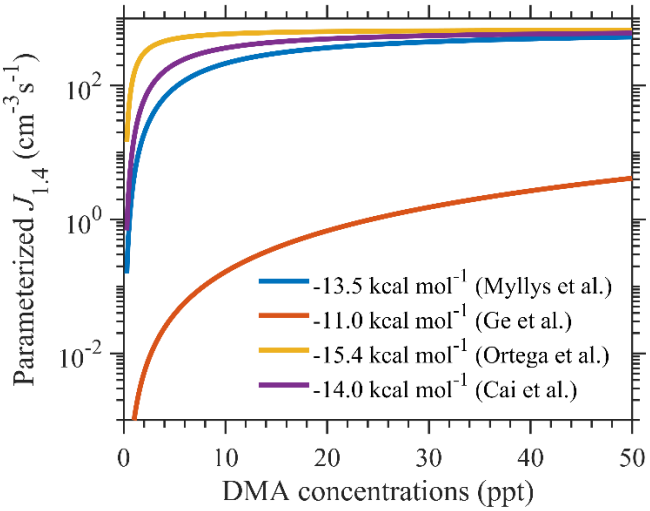

Figure S9. Variation of parameterized J1.4 with DMA concentrations at 281 K with different ΔG values applied of -15.40, -14.00, -13.54, and -11.02 kcal mol-1, respectively.

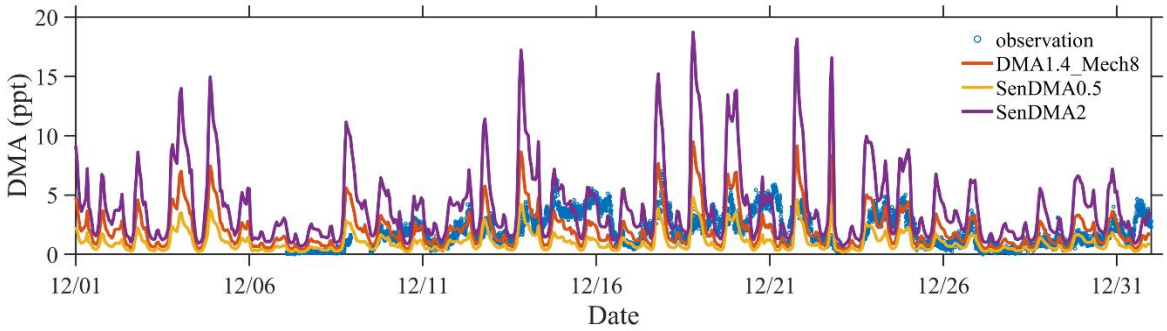

Figure S10. Comparison of observed and simulated DMA concentrations from sensitivity scenarios of halving (SenDMA0.5) and doubling (SenDMA2) the DMA emission and the original scenario (DMA1.4_Mech8).

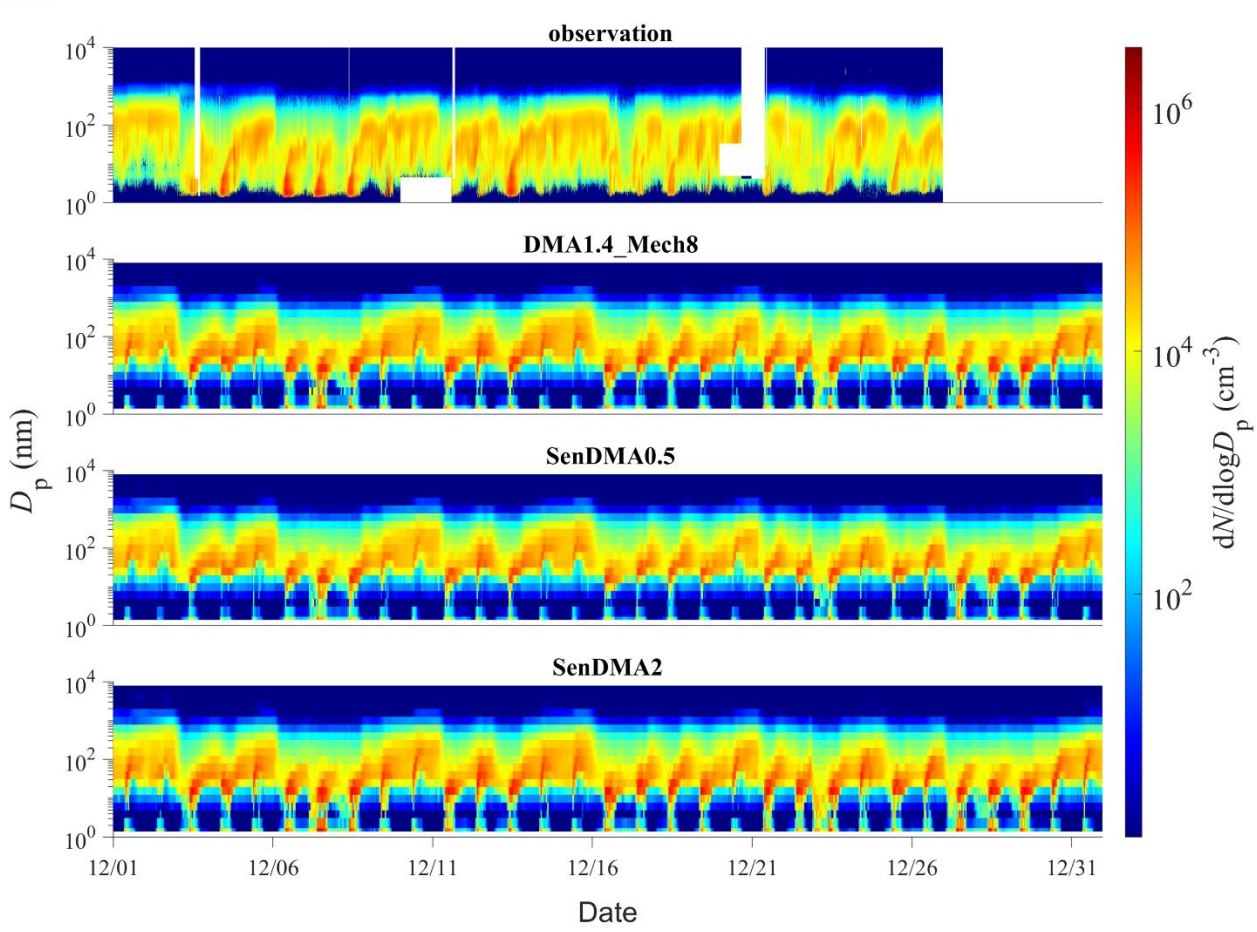

100

101 **Figure S11. Comparison of observed and simulated particle number size distribution from sensitivity scenarios of**
102 **halving (SenDMA0.5) and doubling (SenDMA2) the DMA emission and the original scenario (DMA1.4_Mech8).**

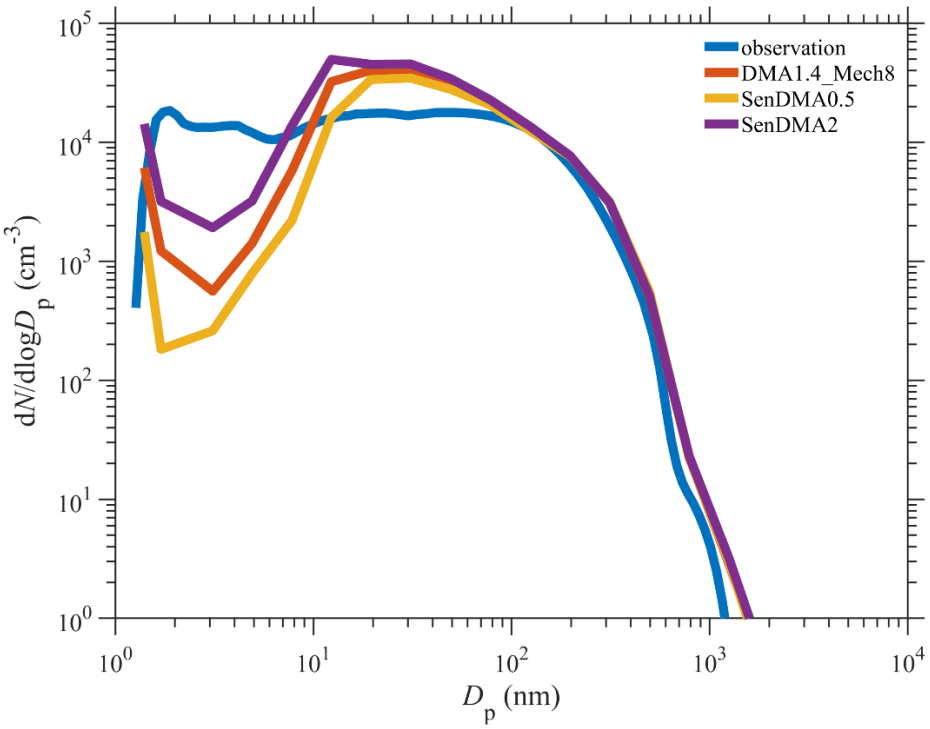

Figure S12. Comparison of observed and simulated averaged particle number size distribution from sensitivity scenarios of halving (SenDMA0.5) and doubling (SenDMA2) the DMA emission and the original scenario (DMA1.4_Mech8).

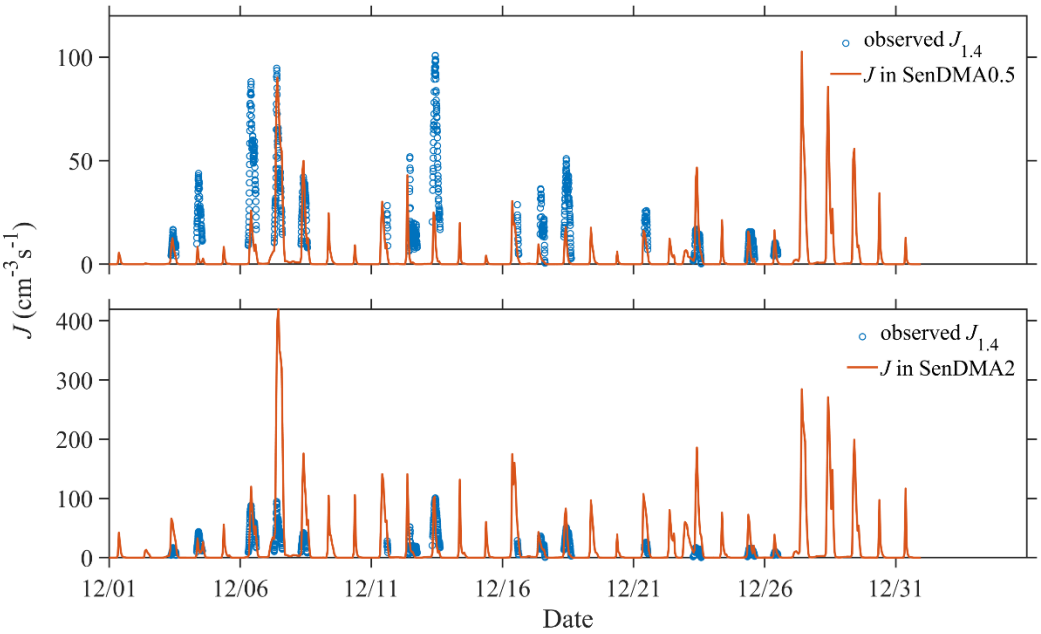

Figure S13. Comparison of observed $J_{1.4}$ and simulated nucleation rate from sensitivity scenarios of halving (SenDMA0.5) (a) and doubling (SenDMA2) (b) the DMA emission.

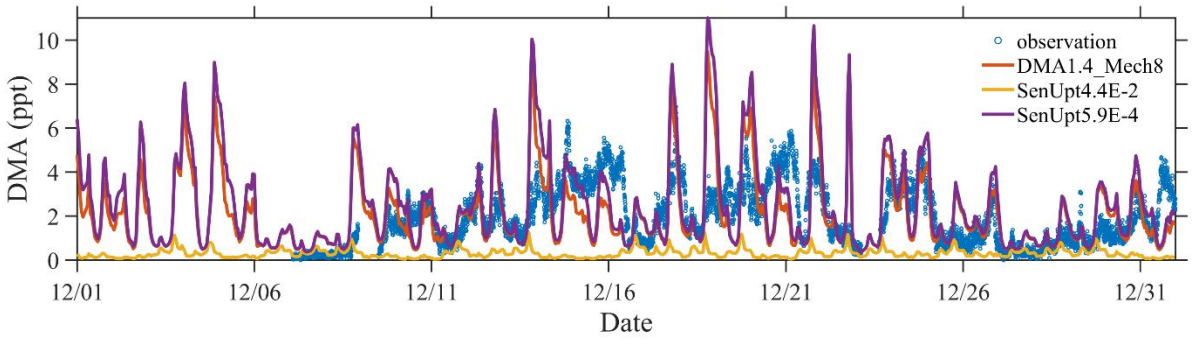

Figure S14. Comparison of observed and simulated DMA concentrations from sensitivity scenarios using lowest (SenUpt5.9E-4) and highest (SenUpt4.4E-2) aerosol uptake coefficient of DMA and the original scenario (DMA1.4_Mech8).

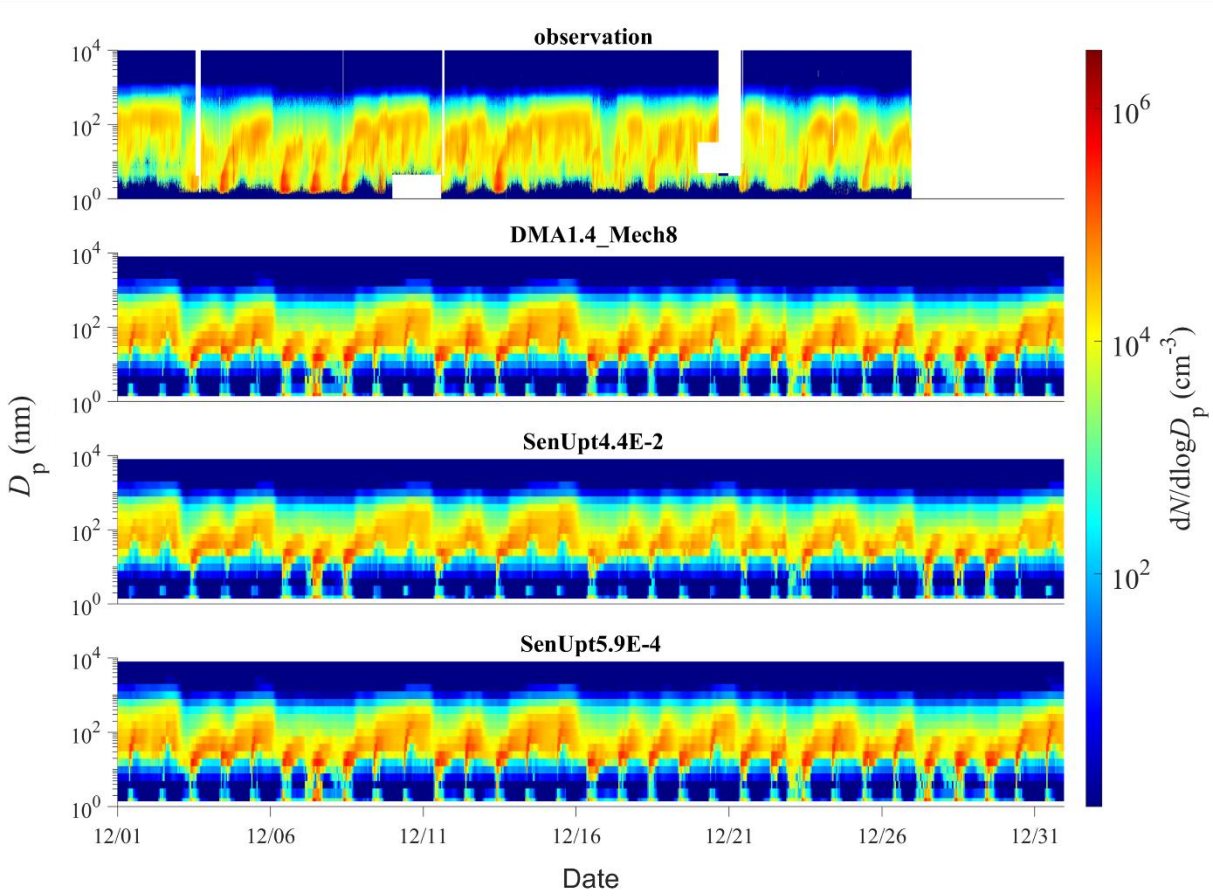

Figure S15. Comparison of observed and simulated particle number size distribution from sensitivity scenarios using lowest (SenUpt5.9E-4) and highest (SenUpt4.4E-2) aerosol uptake coefficient of DMA and the original scenario (DMA1.4_Mech8).

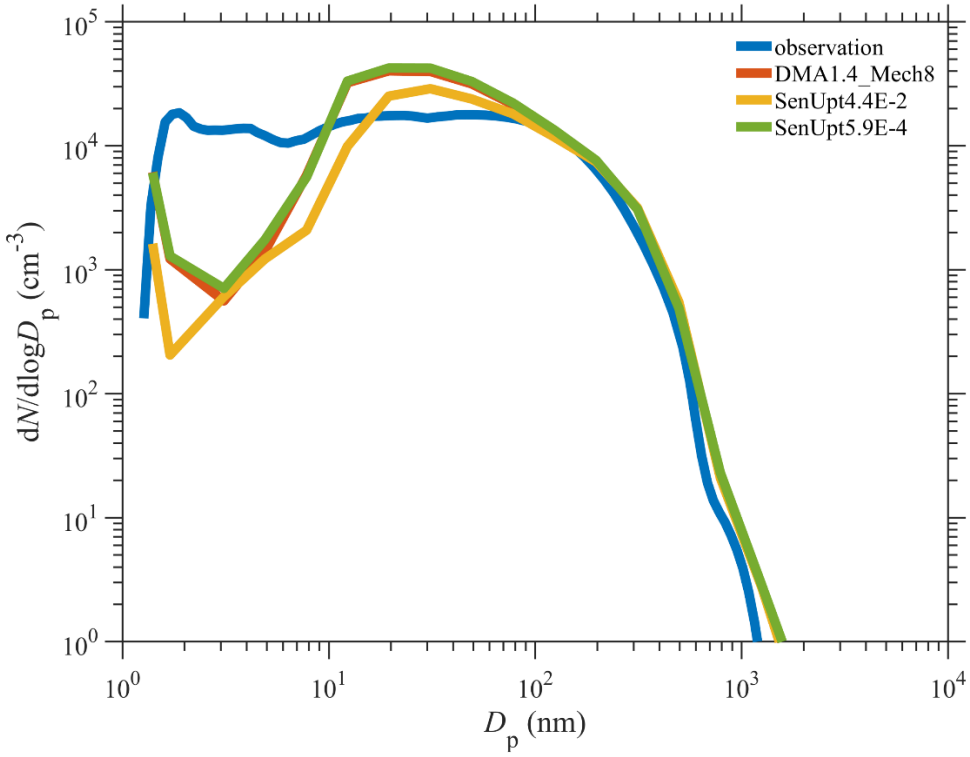

Figure S16. Comparison of observed and simulated averaged particle number size distribution from sensitivity scenarios using lowest (SenUpt5.9E-4) and highest (SenUpt4.4E-2) aerosol uptake coefficient of DMA and the original scenario (DMA1.4_Mech8).

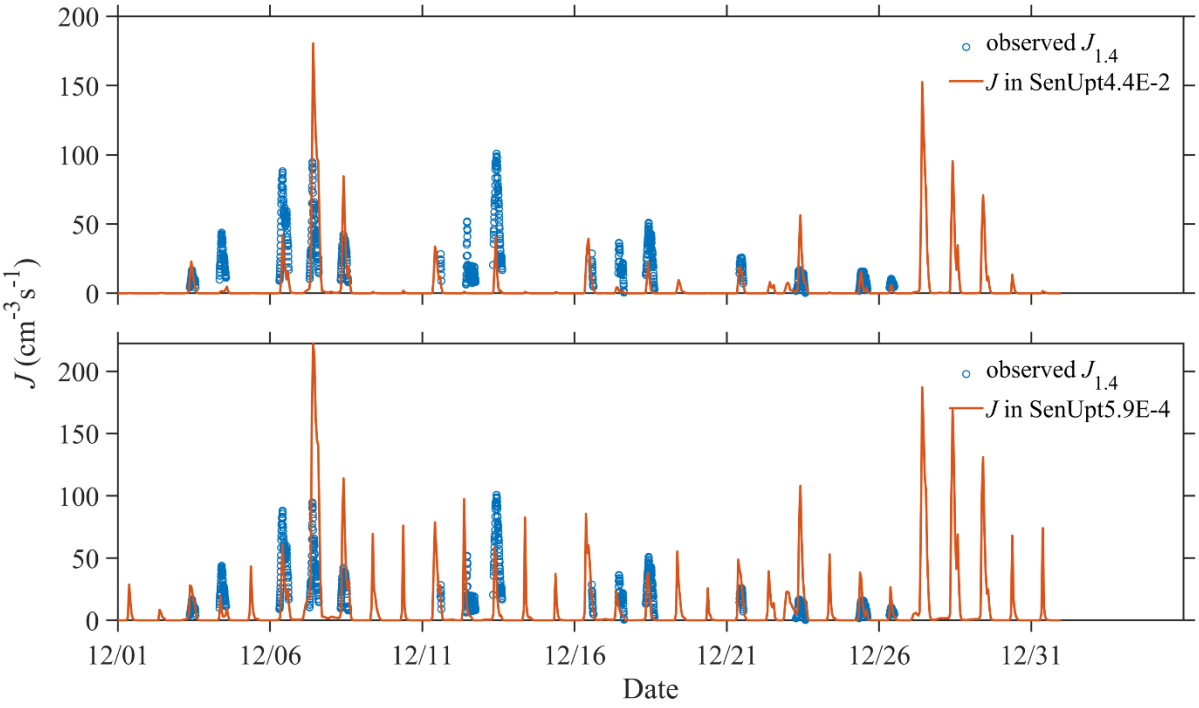

Figure S17. Comparison of observed $J_{1.4}$ and simulated nucleation rate from sensitivity scenarios using lowest (SenUpt5.9E-4) (a) and highest (SenUpt4.4E-2) (b) aerosol uptake coefficient of DMA and the original scenario (DMA1.4_Mech8).

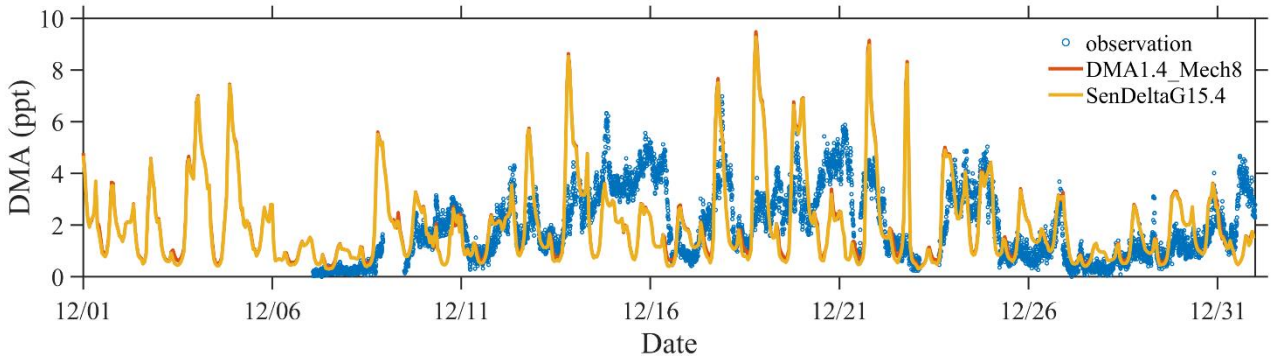

Figure S18. Comparison of observed and simulated DMA concentrations from sensitivity scenarios using ΔG = -15.4 kcal mol^{-1} (SenDeltaG15.4) and the original scenario (DMA1.4_Mech8).

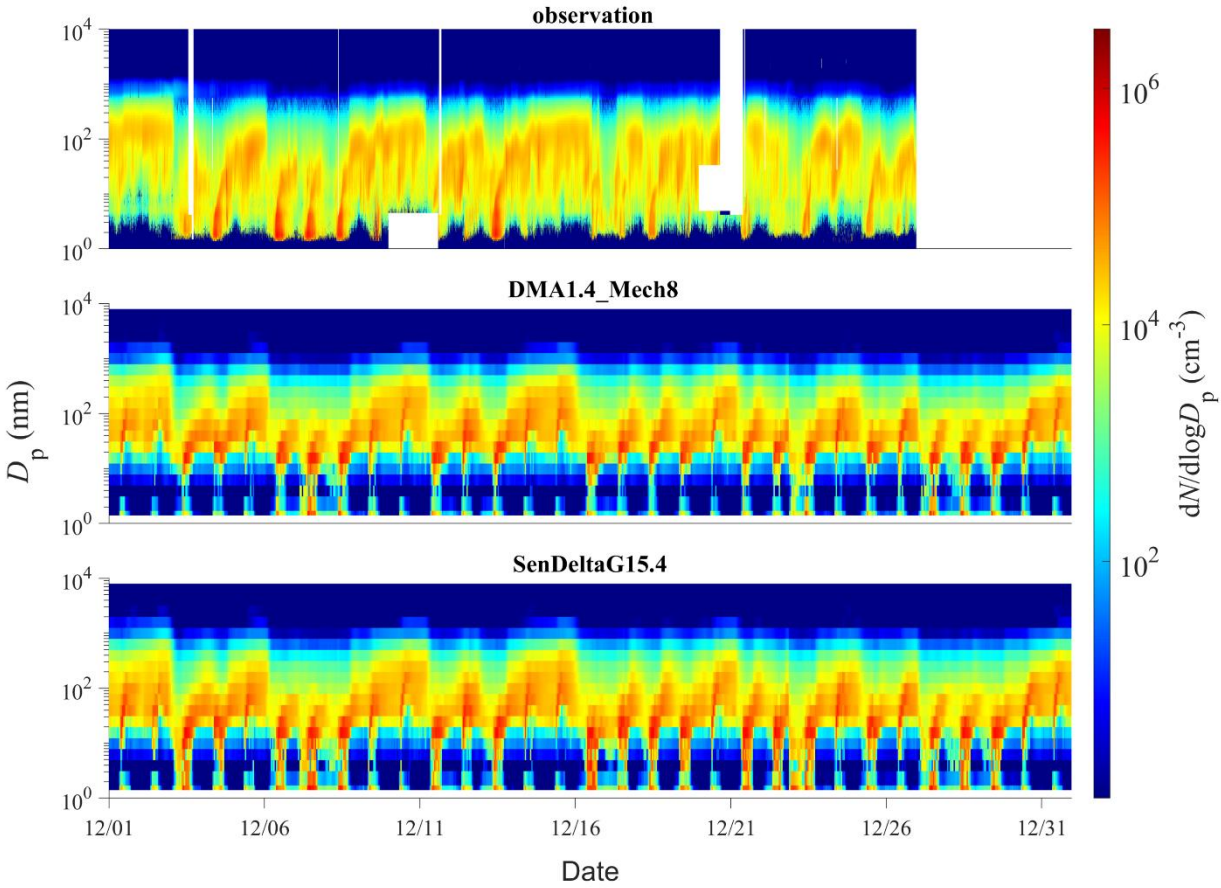

Figure S19. Comparison of observed and simulated particle number size distribution from sensitivity scenario using ΔG = -15.4 kcal mol^{-1} (SenDeltaG15.4) and the original scenario (DMA1.4_Mech8).

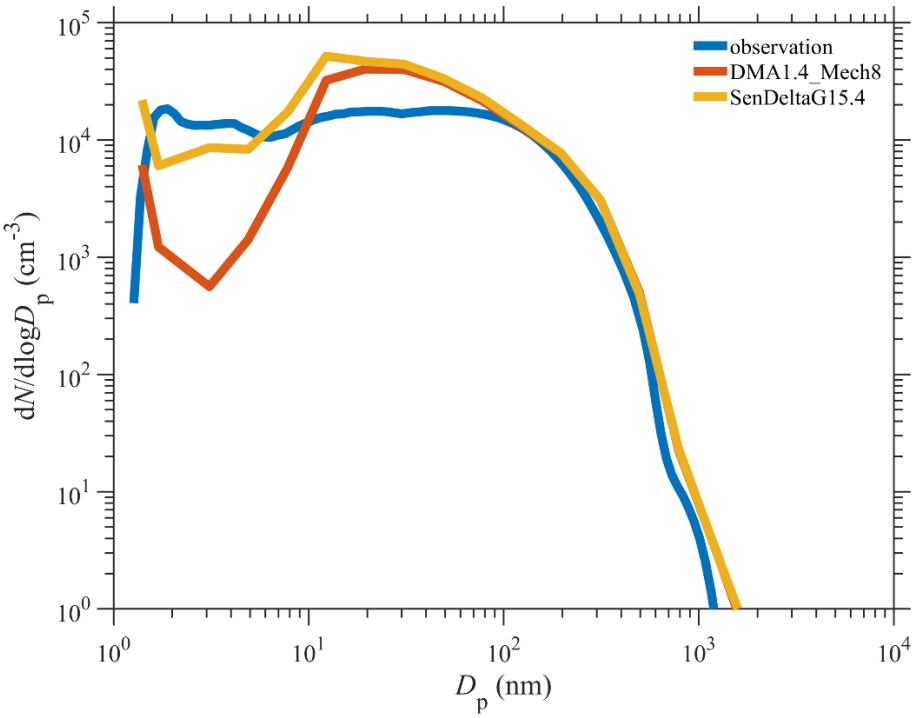

Figure S20. Comparison of observed and simulated averaged particle number size distribution from sensitivity scenarios using ΔG = -15.4 kcal mol^{-1} (SenDeltaG15.4) and the original scenario (DMA1.4_Mech8).

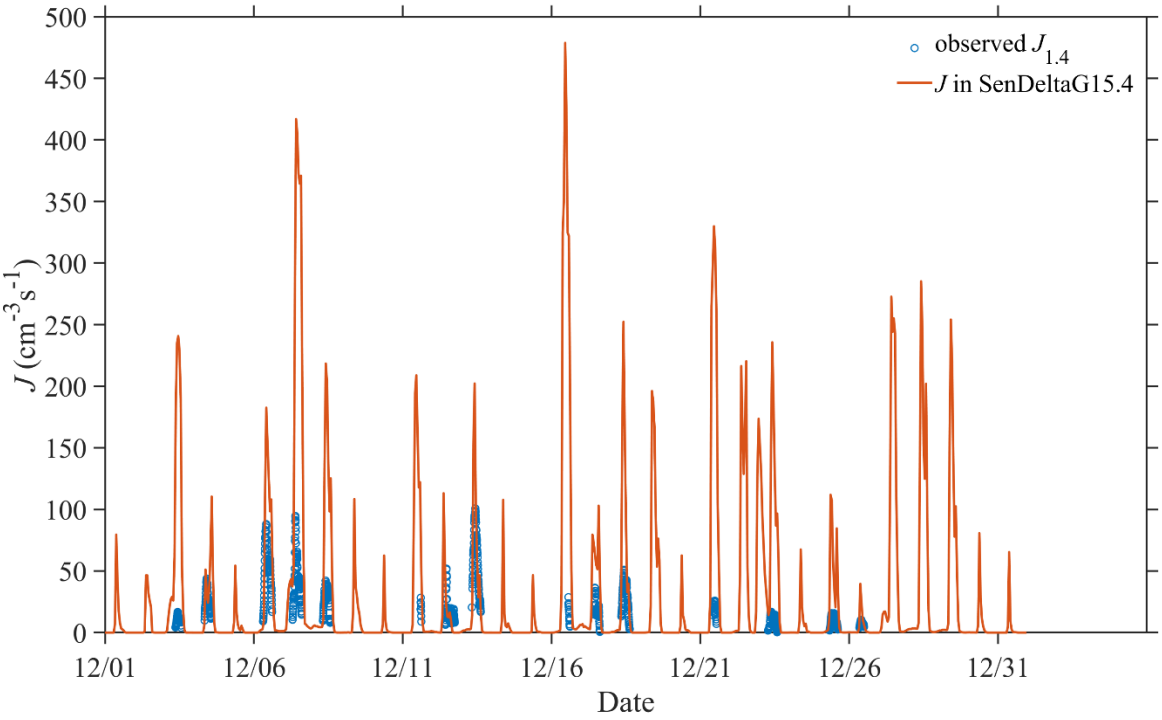

Figure S21. Comparison of observed $J_{1.4}$ and simulated nucleation rates from sensitivity scenarios using ΔG = -15.4 kcal mol^{-1} (SenDeltaG15.4).

References:

Cai, R. L., Yan, C., Yang, D. S., Yin, R. J., Lu, Y. Q., Deng, C. J., Fu, Y. Y., Ruan, J. X., Li, X. X., Kontkanen, J., Zhang, Q., Kangasluoma, J., Ma, Y., Hao, J. M., Worsnop, D. R., Bianchi, F., Paasonen, P., Kerminen, V. M., Liu, Y. C., Wang, L., Zheng, J., Kulmala, M., and Jiang, J. K.: Sulfuric acid-amine nucleation in urban Beijing, Atmos Chem Phys, 21, 2457-2468, 2021.

Carl, S. A. and Crowley, J. N.: Sequential Two (Blue) Photon Absorption by NO_2 in the Presence of H_2 as a Source of OH in Pulsed Photolysis Kinetic Studies: Rate Constants for Reaction of OH with CH_3NH_2, $(CH_3)_2NH$, $(CH_3)_3N$, and $C_2H_5NH_2$ at 295 K, The Journal of Physical Chemistry A, 102, 8131-8141, 10.1021/jp9821937, 1998.

Chen, D., Shen, Y., Wang, J., Gao, Y., Gao, H., and Yao, X.: Mapping gaseous dimethylamine, trimethylamine, ammonia, and their particulate counterparts in marine atmospheres of China's marginal seas – Part 1: Differentiating marine emission from continental transport, Atmos Chem Phys, 21, 16413-16425, 10.5194/acp-21-16413-2021, 2021.

Qiu, C., Wang, L., Lal, V., Khalizov, A. F., and Zhang, R.: Heterogeneous reactions of alkylamines with ammonium sulfate and ammonium bisulfate, Environ Sci Technol, 45, 4748-4755, 10.1021/es1043112, 2011.

Sander, R.: Compilation of Henry's law constants (version 4.0) for water as solvent, Atmos Chem Phys, 15, 4399-4981, 10.5194/acp-15-4399-2015, 2015.

Wang, L., Lal, V., Khalizov, A. F., and Zhang, R.: Heterogeneous Chemistry of Alkylamines with Sulfuric Acid: Implications for Atmospheric Formation of Alkylaminium Sulfates, Environmental Science & Technology, 44, 2461-2465, 10.1021/es9036868, 2010.